REPORT

MANTLE CHEMISTRY

Deep magma ocean formation set the oxidation state of Earth's mantle

Katherine Armstrong*, Daniel J. Frost†, Catherine A. McCammon, David C. Rubie, Tiziana Boffa Ballaran

The composition of Earth's atmosphere depends on the redox state of the mantle, which became more oxidizing at some stage after Earth's core started to form. Through high-pressure experiments, we found that Fe^{2+} in a deep magma ocean would disproportionate to Fe^{3+} plus metallic iron at high pressures. The separation of this metallic iron to the core raised the oxidation state of the upper mantle, changing the chemistry of degassing volatiles that formed the atmosphere to more oxidized species. Additionally, the resulting gradient in redox state of the magma ocean allowed dissolved CO_2 from the atmosphere to precipitate as diamond at depth. This explains Earth's carbon-rich interior and suggests that redox evolution during accretion was an important variable in determining the composition of the terrestrial atmosphere.

Present-day noble gas abundances indicate that impacts caused extensive losses of Earth's proto-atmosphere during accretion (*1*, *2*). A substantial fraction of the atmosphere must therefore have formed by degassing of Earth's interior (*3*, *4*). The oxidation state of the upper mantle during the first 500 million years of Earth's history had a major influence on the composition and evolution of the atmosphere, as it controlled the redox state of degassing volatile species (*5*–*7*). Before Earth's metallic core was fully formed, the mantle was strongly reduced and would have degassed to produce an atmosphere dominated by the reduced gas species CO, CH_4, and H_2 (*7*, *8*). If this state had persisted, these reduced species would have prevented the rise of atmospheric O_2 (*9*). The upper mantle appears, however, to have been substantially more oxidized by the time the first minerals and rocks were formed. Redox conditions are quantified by the oxygen fugacity (f_{O_2}), and f_{O_2} values recorded by the oldest rocks indicate that the redox state of the upper mantle had increased by about 5 log units by the beginning of the geologic record. Subsequent changes appear to have been relatively minor (*10*–*14*). This oxidation event allowed the more oxidized species CO_2 and H_2O to degas from the mantle.

The main mechanism proposed to explain the increase in mantle redox state in the past has been oxidation by H_2O accompanied by the loss of H_2 to space (*8*, *15*). Although this almost certainly occurred to some extent, the question remains as to whether there would be sufficient H_2O left inside Earth after core formation to accomplish this. It is also unclear why Mars, a seemingly more volatile-rich planet than Earth, has an apparently more reduced primitive mantle (*16*–*18*). An alternative oxidation mechanism is based on FeO disproportionation caused by crystallization of bridgmanite, the dominant lower-mantle mineral. Experimental studies show that bridgmanite has a high $Fe^{3+}/\Sigma Fe$ ratio when in equilibrium with iron metal (*19*–*23*). This implies that the equilibrium $3FeO = Fe^0 + 2FeO_{1.5}$, involving ferric and ferrous iron components in mineral phases, shifted to the right as the lower mantle formed. This resulted in the disproportionation of FeO and the precipitation of iron metal (Fe^0). Segregation of precipitated iron metal from the crystallizing lower mantle into the core could have raised the bulk oxygen content of the entire mantle after convective mixing (*19*). We show that the same FeO disproportionation mechanism must occur in silicate liquid at conditions approaching those of the lower mantle, and hypothesize that the increase in the oxidation state of Earth's mantle was an inevitable consequence of the formation of one or more deep magma oceans.

We describe the f_{O_2} of a silicate melt using the equilibrium

$$FeO + \tfrac{1}{4}O_2 = FeO_{1.5} \quad (1)$$

and the expression

$$f_{O_2} = \left(\frac{a_{FeO_{1.5}}^{melt}}{a_{FeO}^{melt} \times K}\right)^4 \quad (2)$$

where a_{FeO}^{melt} is the activity of the FeO component in the silicate melt and K is the equilibrium constant. At ambient pressure, K is such that silicate melts in equilibrium with metallic iron contain negligible Fe_2O_3. For this to change at higher pressures, the volume change for Eq. 1, $\Delta V_{[1]}$, must be negative.

We can determine the sign of $\Delta V_{[1]}$ by examining whether the $Fe^{3+}/\Sigma Fe$ ratio of a silicate melt increases with pressure at a constant temperature and buffered oxygen fugacity. Previous studies performed up to 7 GPa (*24*, *25*) indicated a positive $\Delta V_{[1]}$, which is consistent with the 1-bar volumes and compressibilities (*26*), although it has been proposed that this may change at higher pressures (*27*). We extended these measurements through a series of multianvil experiments to 23 GPa. We chose a relatively polymerized andesitic silicate melt composition to facilitate

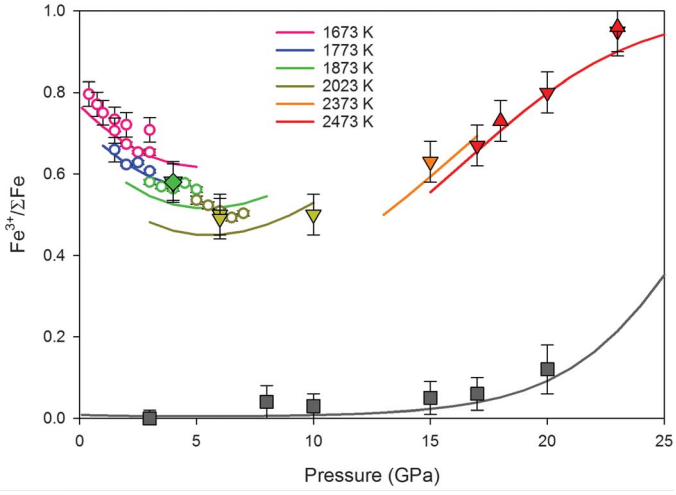

Fig. 1. Ferric iron contents of quenched silicate melts buffered at different oxygen fugacities. We buffered the experimental oxygen fugacity either by the assemblage Ru + O_2 = RuO_2 (colored symbols indicate temperatures), which has an oxygen fugacity of ~ΔIW +8, or by equilibrium with Fe metal (gray squares), ~ΔIW −2. Downward- and upward-pointing triangles indicate initially fully oxidized and fully reduced starting materials, respectively. Results from previous studies are shown as open circles (*24*, *25*). All starting compositions were andesitic except an experiment at 4 GPa that had a MORB melt composition (green diamond). The curves show the fit of our model to the experimental data. The gray curve is calculated for liquid iron metal saturation at 2373 K. The experimental temperature uncertainties are ~50 K.

Bayerisches Geoinstitut, University of Bayreuth, D-95447 Bayreuth, Germany.
*Present address: Peter A. Rock Thermochemistry Laboratory, University of California, Davis, CA, USA.
†Corresponding author. Email: dan.frost@uni-bayreuth.de

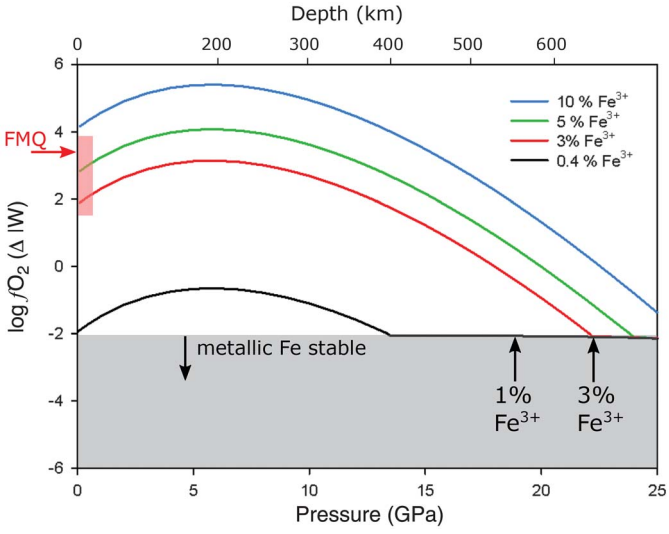

Fig. 2. Magma ocean oxygen fugacity profiles for different bulk $Fe^{3+}/\Sigma Fe$ percentages. We normalized the oxygen fugacity to the iron-wüstite buffer (ΔIW). The value of the FMQ (fayalite, magnetite, quartz) buffer is indicated by the red arrow. The present-day range in upper mantle f_{O_2} is approximated by the vertical red bar. We assume a mantle adiabatic potential temperature of 2273 K. The gray shaded region indicates the f_{O_2} where metallic iron precipitates. Metallic iron precipitation buffers the oxygen fugacity, flattening it with increasing pressure. A magma ocean containing initially only 0.4% ferric iron will start to precipitate metallic iron at ~400 km. If the metal separates to the core, the ferric iron content of the magma ocean will rise to values indicated by the vertical arrows. Once the ferric iron content of the magma ocean reaches 3%, the near-surface f_{O_2} is within the range for the present-day mantle.

glass formation when quenching at high pressures. We used two starting compositions so that we could approach the equilibrium $Fe^{3+}/\Sigma Fe$ ratio both from an initially more oxidized and a more reduced composition. We equilibrated melts with a Ru-RuO_2 buffer, placed in the sample capsule, that resulted in an f_{O_2} approximately 8 log units above the iron-wüstite oxygen buffer (ΔIW +8). The relatively high f_{O_2} makes the measurements more reliable and is not problematic because $\Delta V_{[1]}$ should be independent of f_{O_2}.

After equilibration at high pressure, we analyzed the $Fe^{3+}/\Sigma Fe$ ratios of the quenched silicate melts using Mössbauer spectroscopy. Above 10 GPa, the silicate melt crystallized upon quenching instead of forming a glass. We assumed that the $Fe^{3+}/\Sigma Fe$ ratios of the silicate melts were unmodified by crystallization. The $Fe^{3+}/\Sigma Fe$ ratios we determined near the boundary between glass and crystallized melts were similar, and we did not have any multivalent elements in large enough concentrations to cause major changes in speciation through electron exchange during quenching (*28*).

We found an initial decrease in the $Fe^{3+}/\Sigma Fe$ ratio with increasing pressure (Fig. 1), consistent with a positive $\Delta V_{[1]}$, but the trend reversed above 10 GPa, indicating a negative $\Delta V_{[1]}$. We rationalized this behavior as being due to the compressibility of the Fe_2O_3 melt component becoming greater than that of FeO at high pressure. This could be caused by a pressure-induced change in coordination of Fe^{3+} in the melt (*7*, *29*). We fit the data with a thermodynamic expression for Eq. 1 that describes the $Fe^{3+}/\Sigma Fe$ ratio of the melt as a function of temperature, pressure, f_{O_2}, and melt composition (*24*, *30*). We used a modified third-order Tait equation of state (*31*, *32*) to describe the volumes of the iron oxide components in the melt, allowing us to fit a model to the pressure dependence of the $Fe^{3+}/\Sigma Fe$ ratio (*28*) by refining the iron components' bulk moduli and their pressure derivatives. We tested for the effects of melt composition by performing an experiment at 4 GPa on a mid-ocean ridge basalt (MORB) composition. The resulting melt had an $Fe^{3+}/\Sigma Fe$ ratio almost identical to that of the andesitic melt at the same conditions, which is consistent with predictions (*24*, *30*). We also performed additional experiments at low oxygen fugacities by equilibrating andesitic melts with iron metal. We found constant low $Fe^{3+}/\Sigma Fe$ ratios within error up to 10 GPa, but an increase at higher pressures. Our thermodynamic model reproduces these data well, demonstrating that $\Delta V_{[1]}$, which governs the pressure dependence of the melt $Fe^{3+}/\Sigma Fe$, is essentially independent of f_{O_2}. The increase in Fe_2O_3 stability above 10 GPa results in a substantial proportion of Fe_2O_3 in the melt when in equilibrium with metallic iron. This means that a melt with a negligible Fe_2O_3 content that is transported to pressures above 10 GPa must precipitate iron metal to produce the appropriate equilibrium Fe_2O_3 melt content through the oxidation of FeO.

The accretion of planetary embryos through giant impacts likely resulted in multiple phases of extensive or even complete melting of the proto-Earth (*33*–*36*). We used our model to calculate f_{O_2} as a function of depth though a magma ocean (Fig. 2) created by such a giant impact, by assuming that vigorous convection (*37*, *38*) produced a well-mixed magma with a homogeneous $Fe^{3+}/\Sigma Fe$ ratio. We performed the calculation for a bulk silicate Earth composition, which resulted in a small shift in the f_{O_2}–$Fe^{3+}/\Sigma Fe$ relationship for the melt relative to the andesitic melts due to changes in the activities of the iron components (*28*).

To calculate f_{O_2} as a function of depth, we first take the hypothetical case of an initially reduced magma ocean that is in equilibrium with Fe metal near the surface (Fig. 2). Such a magma ocean would have an $Fe^{3+}/\Sigma Fe$ ratio of ~0.004 and an f_{O_2} of approximately ΔIW −2. For simplicity, we have ignored the effect of Ni, which would raise the f_{O_2} of metal iron equilibrium by up to 1 log unit by forming a Ni-Fe metallic liquid (*28*). For this constant $Fe^{3+}/\Sigma Fe$ ratio, the melt f_{O_2} initially increases slightly with increasing depth and is no longer metal-saturated until 200 km, where the trend reverses because of the sign change of $\Delta V_{[1]}$. Below 400 km, the f_{O_2} of the magma reaches a value at which metallic iron is again stable. At this depth, FeO would disproportionate and precipitate iron metal in order to reach the equilibrium Fe_2O_3 content. With increasing pressure, the negative sign of $\Delta V_{[1]}$ implies that both metal and Fe_2O_3 are produced and the melt $Fe^{3+}/\Sigma Fe$ ratio increases, while the f_{O_2} of the melt flattens out as a result of buffering by iron metal.

If the precipitated metal segregates to the core, the net result is an increase in the Fe_2O_3 content of the silicate liquid. The separation of 0.1 weight percent metal to the core, followed by convective homogenization, would raise the $Fe^{3+}/\Sigma Fe$ of the magma to 0.03 (Fig. 2), which is close to estimates of the present-day mantle (*39*). Greater $Fe^{3+}/\Sigma Fe$ ratios may well have been reached through the separation of more iron metal to the core from progressively greater magma ocean depths, as the ratio of 0.03 estimated for the present-day upper mantle is probably lower than that of the bulk silicate Earth.

Our model shows that for a constant $Fe^{3+}/\Sigma Fe$ ratio, maintained by convection, a gradient in melt f_{O_2} with depth is established. A melt with a ratio of 0.03 remains in equilibrium with metallic iron at lower mantle depths but has an f_{O_2} consistent with the degassing of CO_2 and H_2O near the surface (>ΔIW +2). The f_{O_2} gradient is similar to that proposed for the present-day mantle, which may also reach iron metal saturation at a similar depth (*40*). This is supported by recent observations of iron metal–rich inclusions in gem-quality diamonds that formed between 400 and 660 km depth (*41*).

The removal of metal produced by FeO disproportionation may have raised the $Fe^{3+}/\Sigma Fe$ ratio of the mantle even before core formation was complete. Equilibration with core-forming metal during accretion would have reduced mantle $Fe^{3+}/\Sigma Fe$ ratios to very low values. If the later stages of Earth's accretion, starting from a planetary embryo (i.e., a Mars-size body), occurred mainly through multiple giant collisions (*33*–*36*), FeO disproportionation within each of the resulting magma oceans would have raised the $Fe^{3+}/\Sigma Fe$ ratio of the mantle once the impactor's core had fully segregated. This implies that a H_2O- and CO_2-dominated atmosphere may have been maintained throughout the final stages of accretion. On the other hand, magma oceans on smaller bodies such as the Moon, Mars,

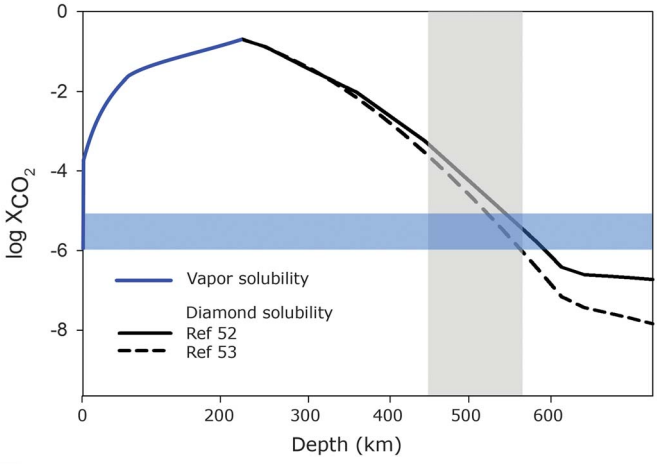

Fig. 3. Carbon dioxide concentration in a magma ocean in equilibrium with diamond. The CO_2 content (in mole fraction) of a CO_2 vapor–saturated melt is shown by the blue curve (*52*); the black curves show the CO_2 content of a diamond-saturated melt, calculated with two different methods (*28*, *52*, *53*). The magma CO_2 concentration is a function of atmospheric CO_2 partial pressure (*7*) but is potentially in the range 1 to 10 ppm, as indicated by the horizontal shaded region. The calculation is performed at 2273 K assuming an oxygen fugacity gradient constrained by a melt with a constant $Fe^{3+}/\Sigma Fe$ ratio of 0.03. The CO_2 content of the melt at diamond saturation drops with depth as f_{O_2} decreases. A melt containing less than 10 ppm CO_2 dissolved at the surface will precipitate diamond at depths of >500 km. The vertical shaded band indicates the approximate conditions, including temperature uncertainty, where diamond is neutrally buoyant in ultramafic melt (*44*, *45*). At depths of >600 km, the melts become saturated in iron metal.

and Vesta were of insufficient depth to cause disproportionation. This explains why their mantles are more reduced [closer to IW (*16*–*18*)], despite Mars forming from more volatile-rich, and therefore potentially more oxidized, material (*42*).

Our experiments were not able to address what happens to the redox conditions in magmas at much higher pressures, which could be relevant for impacts that melted the entire mantle. However, the compressibility of the Fe_2O_3 melt component rivals that of FeO as lower mantle pressures are approached, which may reverse the rising trend in melt $Fe^{3+}/\Sigma Fe$ ratio with pressure. Our model shows some indication of this (Fig. 1) for the more oxidizing conditions. A larger unknown is the impact of electronic spin transitions involving both iron oxide components that could potentially influence the melt $Fe^{3+}/\Sigma Fe$ ratio. These uncertainties are unlikely to negate the effect of FeO disproportionation, even if the latter were restricted to a depth interval near the top of the lower mantle, because the entire magma ocean would pass through this region as a result of convection. The metal produced would ultimately sink to the core, and the increase in Fe_2O_3 would be redistributed to the mantle as a whole through convective mixing.

A gradient in f_{O_2} through a deep magma ocean has been proposed (*7*) to result in a "carbon pump" mechanism that continuously removed small amounts of CO_2 from the overlying atmosphere by dissolution in the magma and subsequent precipitation as diamond in the interior. As Earth experienced a late (Moon-forming) giant impact, this carbon pump might have been important for moving CO_2 from the atmosphere into the mantle. This may explain why, in contrast to other volatile elements such as H and N, a substantial portion of Earth's carbon resides in the mantle (*43*). The carbon pump would operate because a magma ocean in equilibrium with a CO_2-rich atmosphere would still dissolve a few parts per million of CO_2 (*43*). The CO_2 concentration at which the melt reaches carbon (graphite/diamond) saturation, however, would decrease with decreasing f_{O_2} and therefore with depth. This is illustrated in Fig. 3, where we calculate this CO_2 concentration for a magma ocean with an $Fe^{3+}/\Sigma Fe$ of 0.03. As a result of the decrease in f_{O_2}, the CO_2 content of the melt in equilibrium with diamond drops to below 10 ppm at >500 km depth. At such depths, excess carbon would precipitate as diamond and would be neutrally buoyant (*44*, *45*). With time, the diamond content of the mantle would rise, even if the concentration of CO_2 carried by the melt from the surface was low. Venus, on the other hand, may have developed a more CO_2-rich atmosphere because it had not experienced a late giant impact and deep magma ocean formation in which the carbon pump could operate (*46*).

The increase in the oxidation state of the mantle before the end of accretion would also have influenced the conditions under which siderophile (iron metal–loving) elements partitioned into the core, particularly for impactors that were too small to influence mantle f_{O_2}. FeO disproportionation would create an oxidized upper mantle in which small amounts of accreting metal would dissolve. Metal would, however, precipitate again toward lower mantle depths. Siderophile element partitioning would then take place at high pressures and the most oxidizing conditions possible for metal-silicate equilibration in Earth. This may have been important for controlling the proportion of volatile elements that partitioned into the core, particularly if they were delivered predominantly toward the end of accretion (*47*). Earth's apparent depletion of nitrogen might be explained, for example, because it becomes siderophile under such conditions (*48*–*50*). The separation of metal formed through disproportionation would have also prevented highly siderophile elements from becoming overabundant in the silicate Earth toward the final stages of core formation (*51*).

REFERENCES AND NOTES

1. H. E. Schlichting, S. Mukhopadhyay, *Space Sci. Rev.* **214**, 34 (2018).
2. H. Genda, Y. Abe, *Nature* **433**, 842–844 (2005).
3. J. M. Tucker, S. Mukhopadhyay, *Earth Planet. Sci. Lett.* **393**, 254–265 (2014).
4. H. Lammer *et al.*, *Astron. Astrophys. Rev.* **26**, 2 (2018).
5. L. R. Kump, J. F. Kasting, M. E. Barley, *Geochem. Geophys. Geosyst.* **2**, 2000GC000114 (2001).
6. L. Schaefer, B. Fegley Jr., *Icarus* **186**, 462–483 (2007).
7. M. M. Hirschmann, *Earth Planet. Sci. Lett.* **341–344**, 48–57 (2012).
8. J. F. Kasting, D. H. Eggler, S. P. Raeburn, *J. Geol.* **101**, 245–257 (1993).
9. D. C. Catling, M. W. Claire, *Earth Planet. Sci. Lett.* **237**, 1–20 (2005).
10. D. Canil, *Nature* **389**, 842–845 (1997).
11. J. W. Delano, *Orig. Life Evol. Biosph.* **31**, 311–341 (2001).
12. D. Trail, E. B. Watson, N. D. Tailby, *Nature* **480**, 79–82 (2011).
13. S. Aulbach, V. Stagno, *Geology* **44**, 751–754 (2016).
14. R. W. Nicklas *et al.*, *Geochim. Cosmochim. Acta* **250**, 49–75 (2019).
15. Z. D. Sharp, F. M. McCubbin, C. K. Shearer, *Earth Planet. Sci. Lett.* **380**, 88–97 (2013).
16. C. D. K. Herd, L. E. Borg, J. H. Jones, J. J. Papike, *Geochim. Cosmochim. Acta* **66**, 2025–2036 (2002).
17. M. Wadhwa, *Rev. Mineral. Geochem.* **68**, 493–510 (2008).
18. E. A. Pringle, P. S. Savage, J. Badro, J.-A. Barrat, F. Moynier, *Earth Planet. Sci. Lett.* **373**, 75–82 (2013).
19. D. J. Frost *et al.*, *Nature* **428**, 409–412 (2004).
20. Y. Nakajima, D. J. Frost, D. C. Rubie, *J. Geophys. Res.* **117**, B08201 (2012).
21. A. Rohrbach *et al.*, *Nature* **449**, 456–458 (2007).
22. S.-H. Shim *et al.*, *Proc. Natl. Acad. Sci. U.S.A.* **114**, 6468–6473 (2017).
23. D. Andrault *et al.*, *Geochem. Perspect. Lett.* **6**, 5–10 (2018).
24. H. S. C. O'Neill *et al.*, *Am. Mineral.* **91**, 404–412 (2006).
25. H. L. Zhang, M. M. Hirschmann, E. Cottrell, A. C. Withers, *Geochim. Cosmochim. Acta* **204**, 83–103 (2017).
26. V. C. Kress, I. S. E. Carmichael, *Contrib. Mineral. Petrol.* **108**, 82–92 (1991).
27. L. Schaefer, L. T. Elkins-Tanton, *Philos. Trans. R. Soc. A.* **376**, 20180109 (2018).
28. See supplementary materials.
29. Q. Liu, R. A. Lange, *Am. Mineral.* **91**, 385–393 (2006).
30. K. D. Jayasuriya, H. St. C. O'Neill, A. J. Berry, S. J. Campbell, *Am. Mineral.* **89**, 1597–1609 (2004).
31. Y. K. Huang, C. Y. Chow, *J. Phys. D* **7**, 2021–2023 (2002).
32. T. J. B. Holland, R. Powell, *J. Metamorph. Geol.* **29**, 333–383 (2011).
33. W. B. Tonks, H. J. Melosh, *J. Geophys. Res.* **98**, 5319–5333 (1993).
34. J. de Vries *et al.*, *Prog. Earth Planet. Sci.* **3**, 7 (2016).
35. C. B. Agnor, R. M. Canup, H. F. Levison, *Icarus* **142**, 219–237 (1999).
36. L. T. Elkins-Tanton, *Annu. Rev. Earth Planet. Sci.* **40**, 113–139 (2012).
37. Y. S. Solomatov, in *Origin of the Earth and Moon*, R. Canup, K. Righter, Eds. (Univ. of Arizona Press, 2000), pp. 323–338.
38. D. C. Rubie, H. J. Melosh, J. E. Reid, C. Liebske, K. Righter, *Earth Planet. Sci. Lett.* **205**, 239–255 (2003).
39. A. B. Woodland, J. Kornprobst, A. Tabit, *Lithos* **89**, 222–241 (2006).
40. D. J. Frost, C. A. McCammon, *Annu. Rev. Earth Planet. Sci.* **36**, 389–420 (2008).
41. E. M. Smith *et al.*, *Science* **354**, 1403–1405 (2016).
42. G. Dreibus, H. Wänke, *Icarus* **71**, 225–240 (1987).
43. M. M. Hirschmann, *Earth Planet. Sci. Lett.* **502**, 262–273 (2018).
44. E. Ohtani, M. Maeda, *Earth Planet. Sci. Lett.* **193**, 69–75 (2001).
45. A. Suzuki, E. Ohtani, T. Kato, *Science* **269**, 216–218 (1995).
46. S. A. Jacobson, D. C. Rubie, J. Hernlund, A. Morbidelli, M. Nakajima, *Earth Planet. Sci. Lett.* **474**, 375–386 (2017).

47. M. Schönbächler, R. W. Carlson, M. F. Horan, T. D. Mock, E. H. Hauri, *Science* **328**, 884–887 (2010).
48. B. Marty, *Earth Planet. Sci. Lett.* **313–314**, 56–66 (2012).
49. M. Roskosz, M. A. Bouhifd, A. P. Jephcoat, B. Marty, B. O. Mysen, *Geochim. Cosmochim. Acta* **121**, 15–28 (2013).
50. C. Dalou, M. M. Hirschmann, A. von der Handt, J. Mosenfelder, L. S. Armstrong, *Earth Planet. Sci. Lett.* **458**, 141–151 (2017).
51. D. C. Rubie *et al*., *Science* **353**, 1141–1144 (2016).
52. B. Guillot, N. Sator, *Geochim. Cosmochim. Acta* **75**, 1829–1857 (2011).
53. M. S. Duncan, R. Dasgupta, K. Tsuno, *Earth Planet. Sci. Lett.* **466**, 115–128 (2017).

ACKNOWLEDGMENTS

We thank D. Krauße for assistance with EPMA, and H. Schulze, R. Njul, and A. Rother for sample preparation. Discussions with L. Schaefer and M. Hirschmann are greatly appreciated. **Funding:** Supported by the DFG-SPP program 1833 "Building a Habitable Earth" through grant FR 1555/10-1 and through the DFG international research and training group "Deep Volatile Cycles," GRK 2156/1. **Author contributions:** D.J.F. and D.C.R. conceived the project. K.A. performed experiments, analyzed data, and derived the thermodynamic model. C.M. collected and analyzed Mössbauer spectra. T.B.B. collected and analyzed XRD data. K.A. and D.J.F. wrote the manuscript. **Competing interests:** Authors declare no competing interests. **Data and materials availability:** All data are available in the main text or the supplementary materials.

SUPPLEMENTARY MATERIALS

science.sciencemag.org/content/365/6456/903/suppl/DC1
Materials and Methods
Supplementary Text
Figs. S1 to S7
Tables S1 to S6
References (*54*–*75*)

26 April 2019; accepted 2 August 2019
10.1126/science.aax8376

Deep magma ocean formation set the oxidation state of Earth's mantle

Katherine Armstrong, Daniel J. Frost, Catherine A. McCammon, David C. Rubie and Tiziana Boffa Ballaran

Science **365** (6456), 903-906.
DOI: 10.1126/science.aax8376

Deep divide in fate of iron

A large component of Earth's atmosphere comes from the interior, where the gas species are dictated by the redox state of the mantle. After formation of Earth's iron core, the mantle became several orders of magnitude more oxidized. Armstrong *et al.* conducted a set of experiments looking at the redox state of silicate melt representative of Earth's early magma oceans. They found that at some depth, iron oxide disproportionates into iron(III) oxide and metallic iron. The reduced iron sinks to the core, leaving an oxidized rocky mantle that emits carbon dioxide and water instead of more reduced species.

Science, this issue p. 903